How Platinum Oxide Affects the Degradation Analysis of PEM Fuel Cell Cathodes

David Bernhard[a,b,e], Thomas Kadyk[b,c,d], Ulrike Krewer[b,e], Sebastian Kirsch[a,*]

[a] *Volkswagen AG, Am Krainhop 5, 38550 Isenbüttel,Germany*
[b] *Institute of Energy and Process Systems Engineering, TU Braunschweig, Franz-Liszt-Straße 35, 38106 Braunschweig, Germany*
[c] *Theory and Computation of Energy Materials (IEK-13), Institute of Energy and Climate Research, Forschungszentrum Jülich GmbH, 52425 Jülich, Germany*
[d] *Jülich Aachen Research Alliance, JARA Energy, Jülich, Germany*
[e] *Institute of Applied Materials (IAM-WET), Karlsruhe Institute of Technology, Adenauerring 20b, 76131 Karlsruhe, Germany Braunschweig, Franz-Liszt-Straße 35, 38106 Braunschweig, Germany*

Abstract

In this work, proton exchange membrane fuel cell cathodes are degraded with accelerated-stress-tests.These PtCo containing cathodes are analyzed at begin-of-life and end-of-test with an dedicated diagnostic procedure. For every individual load point, the oxygen transport resistance and voltage losses due to the formation of platinum oxides were obtained in addition to commonly measured electrochemical surface area, high frequency resistance, as well as cathode ionomer resistance. These data were used to break down the voltage losses into six different contributors. With this break down, performance gains and performance losses were determined at end-of-test. At low current densities, it was found that voltage losses due to degradation are dominated by the loss of specific activity and catalyst surface area - in line with the state-of-the-art knowledge. But by quantifying the losses from platinum oxide formation explicitly, we show that end-of-test an unassigned voltage loss is not only present at highest current densities, but already at low current density. More precisely, the unassigned voltage loss shows a linear increase with decreasing half cell voltage and is independent from the chosen accelerated stress test. As this unassigned loss depends on half cell voltage, it might arise from ionomer adsorption.

Keywords: proton exchange membrane fuel cell, degradation, loss break down, platinum oxide, unassigned voltage loss

*Corresponding author
Email addresses: david.bernhard@volkswagen.de (David Bernhard), t.kadyk@fz-juelich.de (Thomas Kadyk), Ulrike.Krewer@kit.edu (Ulrike Krewer), sebastian.kirsch@volkswagen.de (Sebastian Kirsch)

1. Introduction

The proton exchange membrane fuel cell (PEM-FC) is a promising technology for automotive drivetrain applications [1]. State of the art cathode materials – like the $PtCo$ catalyst on a carbon support – are prone to lifetime limiting degradation under a wide range of relevant operation conditions [1, 2]. Most importantly, degradation arises from cathode degradation. Cathode degradation itself, today, arises majorly from half-cell voltage cycles. These lead on the one hand to the loss of catalyst surface area and on the other hand to support corrosion. Degradation from freezing, over-temperatures and contaminates are less important [3–5]. Accordingly, detailed understanding of this degradation under relevant driving conditions must be gained. Only with this insight, hybridization strategies can be developed in order to reach the necessary fuel cell lifetime targets while using the minimum amount of precious metals.

Conventionally, activity losses are believed to be the root cause for performance losses of PEM-FCs, especially at high cathode loadings [6–11]. For cathodes containing pure platinum as catalyst material, these voltage losses are related to the loss of electrochemical surface area and can be well estimated from the Tafel relation. The electrochemical surface area loss originates from platinum dissolution, Ostwald ripening, particle agglomeration and also from corrosion of the carbon support material. These mechanisms are discussed in a vast number of publications, including some comprehensive reviews [10, 12–15]. However, cathodes containing low amounts of Pt-alloy catalyst can suffer from four additional degradation phenomena.

The first phenomenon is a reduction of the specific activity, caused by a change of the catalyst morphology due to dealloying [16–18]. For example, Pt-based core-shell structures were found to loose specific activity in response to an increasing outer shell thickness arising from metal leaching [19–21].

Besides the impact on activity, dealloying causes also the second phenomenon, namely increased Ohmic losses. These increased Ohmic losses originate from cation contamination of the ionomer, blocking its sulfonic head groups. For example, Cai et al. [22] used Co^{2+} doped membranes (sulfonic site blockage up to 46 %) to investigate the potential influence of leached out cations on the proton conductivity in the membrane and the cathode catalyst layer. They found increasing high frequency resistance and proton transport resistance with increased cation concentration - espe-

cially under dry operating conditions. Accordingly, a cation impact on the proton conductivity in membrane electrode assemblies without ex-situ membrane-doping, especially at low humidity, is not unexpected [23–25]. However,so far no increase of high frequency resistance or proton transport resistance in alloy-containing membrane electrode assemblies was found if cathode cation leaching is the only reason for ionomer contamination [17].[1]

The third phenomenon causing voltage losses in Pt-alloy containing PEM-FC-cathodes with low catalyst-loadings is an increased oxygen mass-transport resistance. This increase can be induced by changes of the catalyst support (carbon corrosion) as well as the loss of electrochemical surface area ($ECSA$) [8, 17]. Carbon corrosion, on the one hand, can reduce the hydrophobicity of the carbon support, which increases the amount of flooding in the catalyst layer under wet operation conditions. Correspondingly, oxygen transport-related voltage losses increase in the presence of liquid water in the cathode electrode [26, 27]. On the other hand, carbon corrosion can also cause a collapse of the support structure, reducing the porosity. This densification of the support material leads to an increase of the transport-related voltage losses even in the absence of liquid water in the cathode [8, 28, 29]. The $ECSA$-based increase of the oxygen transport resistance arises from the ionomer thin film. The thin film overcoats the active sites and provides a resistance to oxygen transfer based on the oxygen flux per active catalyst surface area. Therefore, reducing the surface area is, at a given current density, equivalent to an increase of the local oxygen flux. This results in a larger oxygen mass transport resistance (R_{O2}) [30–33].

The fourth phenomenon is the limitation of the cell performance of membrane electrode assemblies (MEAs) at high current densities. This limitation of yet unclear origin occurs already at begin-of-life, especially when the cathodes have low catalyst loadings [30, 34–36]. The related losses increase drastically during cathode aging [8, 11, 35]. So far, different authors already explored this phenomenon, trying to trace it back either to a changing reaction mechanism at sufficiently low half cell voltage [37, 38] or to an increased oxygen transport resistance [34, 39, 40]. As there is no explicit explanation, the origin of these losses is still under debate. Doubts about the reaction-mechanism hypothesis mainly arise from the harsh increase of the Tafel slope up to several hundreds of mV at high current densities observed in [8, 36]. These slopes are much steeper than the slopes normally

[1] Nevertheless, Papadias et al. cannot sufficiently disprove the hypothetical relevance of cation leaching for increased Ohmic losses, as only polarization data under 100 % relative humidity are reported [17].

reported in literature for a changed reaction mechanism (up to 140 mV/dec.) [25, 38]. Oppositely, the experimentally observed R_{O2}-increase was never strictly linked to these unassigned losses, as an increase would be required that seems far too large to explain the unassigned voltage loss.[2] However, due to the technical inability to measure oxygen transport resistances under the conditions of the polarization curve[3], it was not possible to disregard the hypothetical R_{O2}-increase, yet.

In this work, unassigned voltage losses of unknown origin were obtained as well. However, these losses occur even at low current densities. Linked with these unassigned voltage losses is a shortcoming of all voltages loss analyses so far: the omission of oxide-related performance losses. Although it is clear that $PtOx$ reduces the activity of the catalyst by "poisoning" part of the active sites [17, 38, 41], it also seems plausible that additional electronic resistances arise in the catalyst particles. Fantauzzi et al. and Kirchhoff et al. simulated the cell voltage dependent oxidation of Platinum nanoparticles [42, 43]. Accordingly, surface oxides are already formed at cell voltages as low as 750 mV.[4] If the cell voltage decreases the surface oxides are altered to subsurface / bulk oxides and the electronic resistances increase. Direct evidence for Ohmic losses from oxides is given by Neff et al., as they show the increase of resistivity with increasing oxygen content in $PtOx$ films [46]. Zhu et al. show how the Ohmic in-plane resistance of a polycristalline Pt-film jumps up (and slowly grows afterwards) once the atmosphere is changed from H_2 to air [47]. Ignoring the $PtOx$-related voltage loss results in the following problem: By comparing polarization curves at the begin-of-life (BoL) and end-of-test (EoT) and disregarding the $PtOx$ formation based voltage

[2] According to [11] the oxygen mass-transport-related voltage loss and the R_{O2} can be calculated with the following equations:

$$\eta_{RO2} = \frac{R \cdot T}{F} \cdot \left(\frac{1}{4} + \frac{\gamma}{\alpha}\right) \cdot ln\left(\frac{p_{O2,ch} - \frac{R \cdot T}{4F} \cdot i \cdot R_{O2}}{p_{O2,ch}}\right)$$

$$R_{O2} = \frac{F}{R \cdot T} \cdot \frac{p_{O2,ch}}{i_{lim}}$$

where i_{lim} represents the limiting current of the used MEA. With these equations voltage losses up to several hundreds of mV can only be explained by two fold increase of the R_{O2}. This is only possible if the limiting current decreases drastically to unreasonably low values.

[3] The simple limiting-current-based method requires low cell voltages, at which flooding or overheating of the used MEA can occur, leading to changed conditions compared to those during polarization curve measurements.

[4] The effect of platinum oxide on the degradation of the PEM-FC cathode itself cannot be suppressed arbitrarily [44], as the typical operation window of the cells in PEM-FC vehicles lies between 0.6 and 0.85 V. However, the voltage losses from Platinum oxide can be reduced, e.g. by implying a dynamic operation strategy that contains frequent phases with cell voltages lower than 750 mV to reduce the formatted oxides [45].

losses, it is inherently assumed that losses from $PtOx$ remain constant during degradation. But this assumption is not reasonable due to the strong dependency of $PtOx$ formation on the half cell voltage [42, 43, 48–50], which is reduced as consequence of degradation. Accordingly, the cell voltage at a given current decreases over lifetime due to degradation, the losses from $PtOx$ should also be expected to decrease [48–51].

The aim of these work is to identify, whether the introduced degradation phenomena are influencing the performance of the analyzed MEAs and how the quantification of $PtOx$-related losses affect the interpretation of the degradation analysis of sate of the PEM-FC cathodes. In the following, the new diagnostic procedure, presented in Section 2.2, is implemented to assign voltage losses in polarization curves to $PtOx$, high frequency resistance (HFR), oxygen mass transport resistance (R_{O2}), electrochemical active surface area ($ECSA$), specific activity (SA) and proton transport resistance (R_{H+}). Consequently, this procedure is used in Section 3 to study voltage losses during cathode degradation, whereby the focus in this contribution lies on analyzing the $PtOx$-losses and their influence on the unassigned voltage losses occurring at high current densities. It will be shown that R_{O2} remains constant over life time, while $PtOx$-related losses decrease. Finally, it becomes apparent, that the unassigned voltage loss increases over life time, impacting high and intermediate current densities.

2. Experimental

2.1. Materials and Equipment

Experimental data were gathered using a 5 cm^2 MEA-design based on the studies of Baker and Caulk [52]. A picture of the used flow field and the MEA is provided in the Appendix A. A cathode loading of 0.25 mg_{Pt}/cm^2 $PtCo$ catalyst with a $Pt:Co$ molar ratio of 70:30 in the raw powder, an un-alloyed Pt anode with a loading of 0.05 mg_{Pt}/cm^2, an ionomer with a low equivalent weight and a persulfonic acid based membrane with a thickness of 18 μm were used. For gas diffusion layers Sigracet 25BC were used on both sides, compressed with a pneumatic hardware to a compression in the active area of 1 MPa. All electrochemical data and operation conditions were gathered with a fully automatized single cell test bench from Horiba Fuel Con and an additional external potentiostat (Zahner Zennium).

2.2. Testing

The basic test sequence consists of four parts. It begins with a conditioning procedure, consisting of several step changes in current and voltage, to activate the MEAs. Afterwards the MEAs are characterized at BoL with the developed diagnostic procedure, described in detail below. After the diagnostic procedure, the used MEAs were degraded with accelerated stress tests (AST) [15, 53, 54]. The ASTs were ended after 31500 cycles and the diagnostic procedure was repeated to characterize the MEAs at EoT.

Fig. 1 shows the developed diagnostic procedure. It starts with determining the $ECSA$ using cyclic voltammetry (CV) (Fig.1a). The CVs were recorded with a *Zahner Zennium* between 0.06 and 0.7 V (vs. H_2-anode) under N_2 atmosphere with 20 mV/s and were analyzed to derive $ECSA$ and the H_2 crossover [8, 11]. The electrochemical surface area was obtained by averaging the H-desorption and H-adsorption charge (using a specific charge of 210 $\mathrm{C/cm^2_{Pt}}$). After the CV, the diagnostic procedure shown in Fig. 1b-d is run with a cell temperature of 80 °C, H_2/air flows of 5 Nl/min, an inlet pressure on both sides of 2.0 bar and a relative humidity of 100 % at the cell inlet. With the high stoichiometries (>10 at 1.8 $\mathrm{A/cm^2}$) and the specific flow-field design, it is ensured, that the 5 $\mathrm{cm^2}$-active-area is exposed to differential conditions – gradients along-the-channel in pressure, relative humidity, temperature and/or oxygen partial pressure are negligible.. It consists of 13 different measurement sequences of 15 min, each belonging to a specific current density between 0 and 2.0 $\mathrm{A/cm^2}$. In each sequence different "diagnostic tools" contained in three phases are used to extract the desired cell properties, as depicted in Fig.1c.

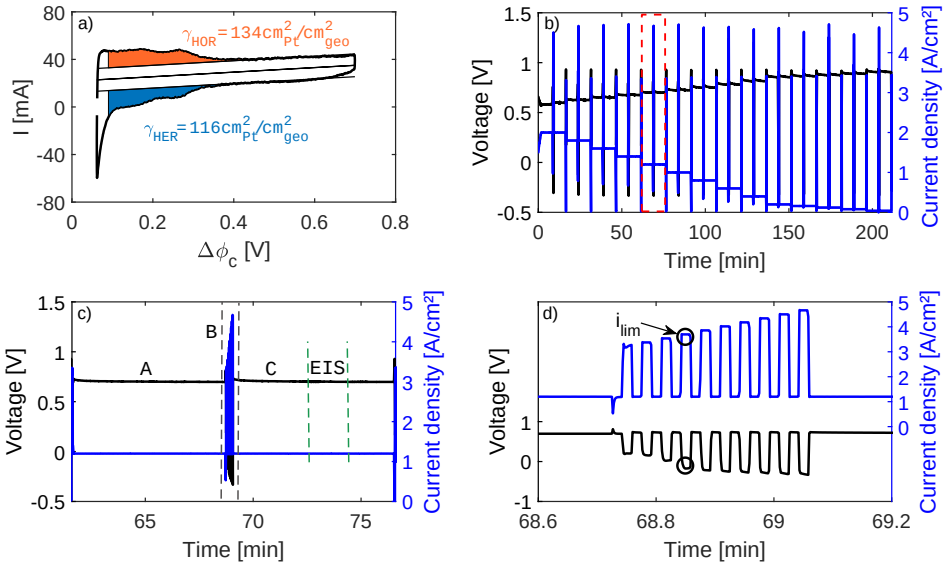

Figure 1: The developed diagnostic procedure: a) Measured CV under N_2 operation for $ECSA$ determination; b) Overview of the developed diagnostic procedure containing the 13 measurement sequences between 2.0 and 0.0 A/cm^2 c) Exemplary sequence showing the the three different phases of the procedure at 1.2 A/cm^2 d) Zoom into the 10 current changes conducted in phase B.

In phase A, the cell is conditioned for 7.5 min at the desired current density to set up the liquid water profiles (in-plane and through-plane) in the MEA (Fig. 1c). In phase B, one potentiostatic and nine galvanostatic steps are carried out. Thereby, during the first step the the voltage of 0.2 V is set for one second and the average current density is measured. Afterwards the steady state current density of phase A is set again for 1 second, followed by nine galvanostatic steps. In these steps the current density measured in the potentiostatic step is increased step-wise to obtain even lower voltages. In each of these steps the high current densities are maintained for 1 second, followed by a 1 second hold at the steady state current density of phase A. The aim of this sequence is two-fold. On the one hand, at these low voltages $PtOx$ is completely reduced. On the other hand, from this sequence the R_{O2} for the load point and its corresponding liquid water profile is estimated. For this estimation, the current density at the reversal point shown in Fig. 1d is used. For more details about the procedure and its legitimization, the reader is referred to [55].

In phase C the current density of phase A is held for another 7.5 mins. Thereby, a voltage decay

is seen that is attributed to the re-formation of $PtOx$. The maximum voltage (∼1 s after the start of phase C) is considered to be "$PtOx$-free".[5] The average voltage of the last two minutes of phase C is referenced as equilibrium voltage. This voltage is used to extract the so-called equilibrium polarization curves from the 13 test sequences shown in Fig. 1b. From the $PtOx$-free and equilibrium voltage, the losses due to $PtOx$-formation can be determined. The strict linkage of the voltage decay in phase C to the formation of $PtOx$ is reasonable as all other potential causes can be ruled out [55]: Firstly, the contribution from double layer charging within in observed voltge decay is insignificant as the capacitive current is in in the range of several μA/cm^2, assuming 100 mF/cm^2 as double layer capacity. Secondly, as phase B is too short to change the temperature of the whole cell setup, the temperature in the catalyst layer and the GDL adapts within 200 ms after the last limiting current measurement and the temperature in phase C is constant. Thirdly if liquid water is absent the rH-profile is also settled within ms after phase B. Consequently, no changes of the Ohmic losses in phase C are expected. Fourthly, the resettling of the oxygen profile after phase C is finished after 25 ms and we assume that the liquid water profile and the mass-transport-related losses within in phase C are constant, too.

Fifthly, if liquid water is present in the GDL and/or cathode electrode, we argue that there is not enough time to evaporate a lot of water and the mass-transport-related losses are also unchanged in phase C. This rationalization of the unchanged liquid water profile over phase C is further supported by our later discussed findings (Fig. 5), that the $PtOx$-losses at BoL are almost independent on current density - a misinterpretation of the mass-transport losses due to varying liquid profiles would cause a notable dependence instead.

In addition to the $PtOx$-loss determination, EIS-Spectra between 50 Hz and 30 kHz are recorded from minute 3 to minute 4.5 of phase C (Fig. 1c). These spectra are then fitted with the help of a transmission line model to derive HFR and R_{H+} according to [56]. A detailed picture of the HFR and R_{H+} determination is given in the Appendix B. In order to estimate the specific catalyst activity (SA), the current density at 0.9 V is estimated by extrapolating the measured $PtOx$-free polarization curve between 0.04 and 0.12 A/cm^2. This current is divided by the derived $ECSA$. After the diagnostic procedure, the used MEAs were degraded with accelerated stress tests (AST)

[5] The term "$PtOx$-free" used in this context is somewhat loosely as in the first second of the hold time some surface adsorbates will have formed.

as summarized in table 1.

Table 1: Operation conditions during the AST including variations of the holdtime at the lower and upper potential limit.

General Operation Conditions		
	Potential shape	Square Wave
	Lower Potential Limit (LPL)	0.6 V
	Upper Potential Limit (UPL)	OCV
	Temperature	90 °C
	Relative Humidity (rH)	100 %
	Inlet Pressure (p_{in})	2.0 bar
	Cycle number	31500
AST-1	Hold time	2.5 s
AST-2	Hold time	10 s
AST-3	Hold time	20 s

The AST consisted of 31500 cycles, with each consisting of potentiostatic steps between open circuit voltage and 0.6 V, with different holding times at each potential. After 31500 AST cycles the diagnostic procedure is carried out again to obtain the desired EoT MEA properties. The complete process containing conditioning, BoL diagnostic, AST and EoT diagnostic was run with two identical cells for AST-1 and 3. In Figure 2, exemplary BoL and EoT polarization curves obtained with the diagnostic procedure are shown for one cell. The solid lines represent the so-called equilibrium polarization curves, while the dashed lines are the $PtOx$ free polarization curves. From the gap between these two types of polarization curves, the influence of $PtOx$ on the cell performance can easily be derived.

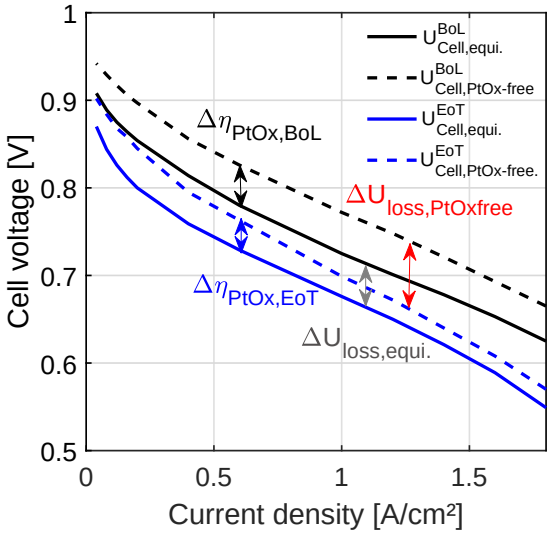

Figure 2: Exemplary polarization data BoL and EoT obtained with the developed diagnostic routine.

2.3. Voltage Loss Break Down

In this section, it is shown how the performance change of the degraded MEA can be broken down into single voltage loss contributions, which are quantified with the gathered data. In Figure 2 the solid black and blue lines represent the measured equilibrium polarization curve at BoL and EoT ($U_{Cell,equi.}^{BoL/EoT}$), respectively. They contain the reversible cell voltage U_{rev} and the various overvoltages:

$$U_{Cell,equi.}^{BoL/EoT} = U_{rev} - \eta_{HFR}^{BoL/EoT} - \eta_{a}^{BoL/EoT} - \eta_{act}^{BoL/EoT} - \eta_{H+}^{BoL/EoT} - \eta_{RO2}^{BoL/EoT} - \eta_{PtOx}^{BoL/EoT} - \eta_{?}^{BoL/EoT} \tag{1}$$

These overpotentials are Ohmic losses, η_{HFR}, related to the proton-transport through the membrane and the Ohmic resistances of the electrically conductive components of the cell, activity losses of the anode, η_a, (neglected in the rest of this work due to high anode activity) and losses related to cathode. These cathode losses are the activation overpotential, η_{act}, losses related to the transport of protons through the cathode η_{H+}, losses attributed to the oxygen transport from the gas channels to the catalyst η_{RO2} and losses related to the formation of surface oxides η_{PtOx}. Furthermore, possible unassigned overpotentials are referred as $\eta_?$. The $PtOx$-free polarization curves is described

by setting η_{PtOx} to zero:

$$U_{Cell,PtOx-free}^{BoL/EoT} = U_{rev} - \eta_{HFR}^{BoL/EoT} - \eta_{a}^{BoL/EoT} - \eta_{act}^{BoL/EoT} - \eta_{H+}^{BoL/EoT} - \eta_{RO2}^{BoL/EoT} - \eta_{?}^{BoL/EoT} \quad (2)$$

As $U_{Cell,equi}^{BoL/EoT}$ and $U_{Cell,PtOx-free}^{BoL/EoT}$ are measured (as described in section 2.2), the $PtOx$ losses are derived from their difference:

$$\eta_{PtOx}^{BoL/EoT} = U_{Cell,PtOx-free}^{BoL/EoT} - U_{Cell,equi}^{BoL/EoT} \quad (3)$$

To quantify the degradation caused performance losses designated as $\Delta U_{loss,equi}$ and $\Delta U_{loss,PtOx-free}$ in Figure 2, the difference between the BoL and EoT polarization is determined as:

$$\Delta U_{loss,equi} = U_{Cell,equi}^{BoL} - U_{Cell,equi}^{EoT} \quad (4)$$

$$\Delta U_{loss,PtOx-free} = U_{Cell,PtOx-free}^{BoL} - U_{Cell,PtOx-free}^{EoT} \quad (5)$$

The obtained differences of the BoL and EoT overpotentials are described in equation 6 and 7:

$$\Delta U_{loss,equi.} = \Delta\eta_{ECSA} + \Delta\eta_{SA} + \Delta\eta_{HFR} + \Delta\eta_{RH+} + \Delta\eta_{RO2} + \Delta\eta_{PtOx} + \Delta\eta_{?} \quad (6)$$

$$\Delta U_{loss,PtOx-free} = \Delta\eta_{ECSA} + \Delta\eta_{SA} + \Delta\eta_{HFR} + \Delta\eta_{RH+} + \Delta\eta_{RO2} + \Delta\eta_{?} \quad (7)$$

The first and the second term of equation 6 account for losses which are related to a reduced $ECSA$ and a changed catalyst activity. For the estimation of these losses the Equations 8-11 are used:

$$\Delta\eta_{act} = \eta_{act}^{BoL} - \eta_{act}^{EoT} = b \cdot log_{10}\left(\frac{i_{0.9V}^{BoL}}{i_{0.9V}^{EoT}}\right) \quad (8)$$

$$\Delta\eta_{ECSA} = b \cdot log_{10}\left(\frac{ECSA^{BoL}}{ECSA^{EoT}}\right) \quad (9)$$

The current density $i_0^{Bol/EoT}$ is obtained from extrapolation (or interpolation) of the $PtOx$-free polarization curve. The $ECSA^{BoL/EoT}$ used in equation 9 stems from CV measurements (see section 2.2). b represents the Tafel slope:

$$b = 2.303 \cdot \frac{R \cdot T}{\alpha \cdot F} \quad (10)$$

With R being the gas constant, T being the cell temperature in Kelvin, α being the cathodic transfer coefficient ($\alpha = 1$ according to [57]) and F being the Faraday constant. Accordingly, the Tafel slope is approximately 70 mV/dec [8, 11, 38]. The losses related to a changed specific activity are calculated with equation 11:

$$\Delta\eta_{SA} = \Delta\eta_{act} - \Delta\eta_{ECSA} \tag{11}$$

The third part of the performance loss is linked to changes of the HFR extracted from the impedance spectroscopy described in section 2.2. This performance loss is described in equation 12:

$$\Delta U_{HFR} = i \cdot A \cdot (HFR^{BoL} - HFR^{EoT}) \tag{12}$$

Where i describes the current density and A the active area of the used MEA (5 cm^2). The fourth contributor to the performance losses is the change of proton conductivity in the cathode. This voltage loss is estimated with equation 13 [56]:

$$\Delta\eta_{H+} = \frac{1}{3} \cdot i \cdot A \cdot (R_{H+}^{BoL} - R_{H+}^{EoT}) \tag{13}$$

Where $R_{H+}^{BoL,EoT}$ is extracted from the impedance spectra (see Appendix Fig. 11). The fifth term of equation 6 is related to the comparison of the mass-transport behavior of the fresh and aged MEA. An equation derived in the work of Zhirul et al. [11] is used to calculate the mass-transport-related voltage loss at end-of-test:

$$\Delta\eta_{RO2} = \frac{R \cdot T}{F} \cdot \left(\frac{1}{4} + \frac{\gamma}{\alpha}\right) \cdot ln\left(\frac{p_{O2,ch} - \frac{R \cdot T}{4F} \cdot i \cdot R_{O2}^{BoL}}{p_{O2,ch} - \frac{R \cdot T}{4F} \cdot i \cdot R_{O2}^{EoT}}\right) \tag{14}$$

Where $R_{O2}^{BoL,EoT}$ is derived from the limiting current measurements described in section 2.2, α represents the cathodic transfer coefficient and γ is the ORR reaction order with respect to oxygen partial pressure ($\gamma = 0.54$ according to [57]). The oxygen partial pressure in the channels of the flow field is described with $p_{O2,ch}$. Equation 15 describes the influence of the sixth term of Equation 6 on the cell performance,

$$\Delta\eta_{PtOx} = \eta_{PtOx}^{EoL} - \eta_{PtOx}^{BoL} \tag{15}$$

The last part of Equation 6 is attributed to unassigned voltage losses introduced in section 1 and is addressed by $\Delta\eta_?$:

$$\Delta\eta_? = \eta_?^{EoL} - \eta_?^{BoL} \tag{16}$$

Whereby $\eta_?^{Bol/EoT}$ is obtained from equation 6, as all other contributors are calculated with the equations 8-15 and the different measured BoL and EoT values are specified. The equations introduced above are valid under the assumption that the cell temperature is constant over the active area and that the difference between the oxygen and hydrogen concentration at the cell in- and outlet is insignificant.

3. Results and Discussion

This section is divided in four parts. In the first three parts the BoL and EoT data gathered with the diagnostic procedure are discussed. In section 3.4 finally, the break down of the EoT performance loss into the different contributors is analyzed.

3.1. High Frequency Resistance, Cathode Proton Transport Resistance and Oxygen Mass-Transport Resistance

Fig. 3 shows the measured HFR, R_{H+} and R_{O2} at low, medium and high current densities. The Fig. 3a-c represent the high frequency resistances derived from the EIS measurements. The differences between the BoL and EoT values are insignificant. Consequently, it can be concluded, that the proton conductivity of the membrane is not significantly reduced, e.g. by leached-out Co^{2+} from the cathode or other membrane degradation effects.

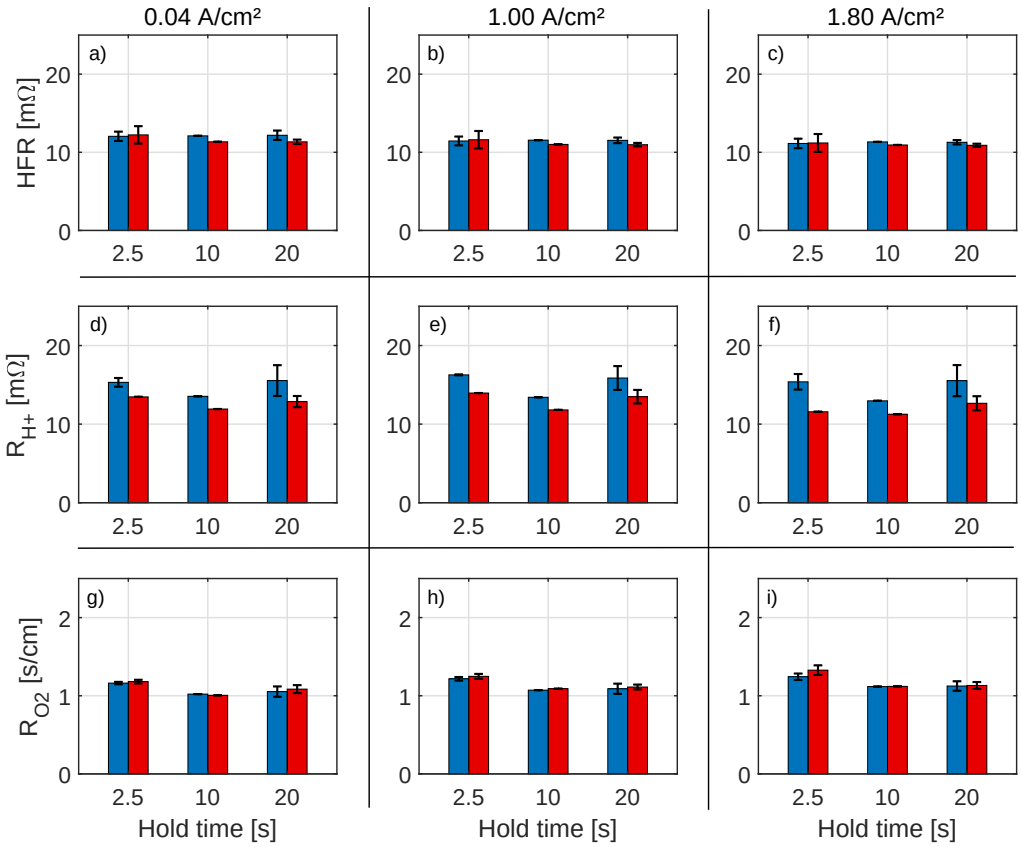

Figure 3: Overview of the measured BoL (blue) and EoT (red) values of HFR (a-c), R_{H+} (d-f) and R_{O2} (g-i) at 0.04, 1.0 and 1.8 A/cm^2 for all three accelerated stress tests (variation of hold times).

The Fig. 3d-f show the obtained R_{H+}. Even though there is a considerable scattering of the data (e.g. compare the BOL values), the proton transport resistance generally decreases at EOT. The reduction of R_{H+} is possibly a result of reduced cathode thickness following carbon corrosion, which is known to become relevant at voltages as high as 0.95 V [35, 58–60]. In addition to the reduced proton transport pathway, the reduced cathode layer thickness leads to an increasing amount of ionomer per volume, resulting in lower values for cathode proton resistance, as discussed, e.g.,in [61, 62]. The influence of the changed cathode layer thickness on the Ohmic behavior of the analyzed MEAs is insignificant, as the HFR is mainly determined by the proton conductivity of the membrane.

In Fig. 3g-l the extracted mass-transport resistances are summarized. For this cathode property the difference between BoL and EoT is also insignificant. This result is in contradiction to the expectation derived from literature, where carbon corrosion leads to an increase of the oxygen mass-transport resistance [28, 29, 35]. But it is in line with findings recently published by Harzer et. al. [8], where carbon corrosion was evident from SEM images although no significant increase in R_{O2} was detected. Generally we observed, no difference in impact of the different degradation procedures on electron, ionic and oxygen mass transport.

3.2. Catalyst Activity

Fig. 4 shows the electrochemical surface area ($ECSA$), current densities at 0.9 V, and the derived specific activity (SA) at BoL and EoT - normalized to the BoL values. The loss of current densities at 0.9 V increases with increasing hold time between 2.5 and 10 s but no significant difference between 10 and 20 s is found (Fig. 4a). These losses can be divided in losses of $ECSA$ and SA. The $ECSA$ losses are shown in Fig. 4b. Comparable results can be found in literature [60, 63], where higher $ECSA$ losses were found with increasing hold times at the upper potential limit and lower potential limit.

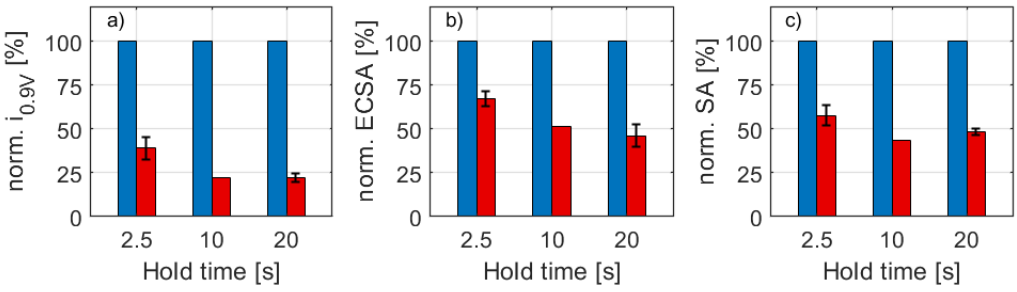

Figure 4: Overview of the normalized current densities at 0.9 V (a), electrochemical surface area (b) and specific activity (c) values at BoL (blue) and EoT (red) for all three accelerated stress tests (variation of hold times).

The loss of SA (Fig. 4c) is a well known degradation phenomenon for alloy catalyst [16, 17, 64, 65]. For pure Pt catalyst or catalyst with a very low alloy content, the specific activity shows only a slight decreases at EoT [17, 66, 67]. Consequently the loss of $ECSA$ determines the voltage losses related to a changed activation overpotential [11, 35]. The loss of SA for PtCo catalyst used in this work can be related to dealloying effects. The loss of the non-precious metal due to degradation

results in a loss of the activity enhancing effect due to altered electronic structure of the catalyst material [17, 65].

3.3. Platinum Oxide Related Overvoltages

In Fig. 5a, the PtOx related overvoltages at BoL and EoT are shown as a function of cell voltage. But as the PtOx formation is driven by the potential on the cathode side it is necessary to consider the PtOx related overvoltages at BoL and EoT as function of half cell potential (Fig. 5b) to avoid a misinterpretation of development of the PtOx related losses over time. The half cell potential is obtained by correcting the measured cell voltage $U_{equi.}^{BoL/EoT}$ with $\eta_{HFR}^{BoL/EoT}$, $\eta_{H+}^{BoL/EoT}$ and $\eta_{RO2}^{BoL/EoT}$. In general, Fig. 5b shows that the PtOx related overvoltages already exist at half cell potentials higher than 720 mV. This is in line with the recently published work of Kirchhoff et al., who show that oxide formation on platinum nanoparticles can already begin at 700 mV [43]. The PtOx related overvoltages increase with increasing half cell potential (decreasing current density) between 750 and approximately 820 mV. After this maximum, the overvoltage decreases as the current density is further reduced.

To interpret this behavior, first, it needs to be said, that to the best of the authors knowledge no

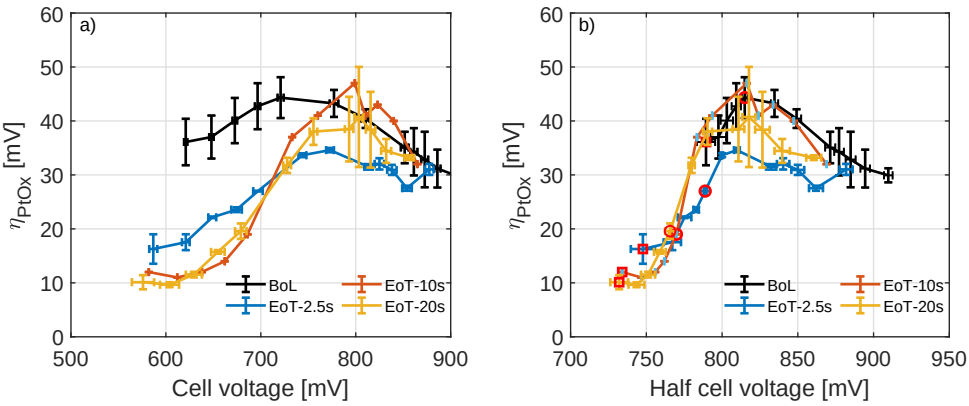

Figure 5: a) η_{PtOx} as function of the cell voltage BoL and EoT; b) η_{PtOx} as function of the half cell potential BoL and EoT (red circles: $\eta_{PtOx}^{BoL/EoT}$ @ 1.0 A/cm^2, red squares: $\eta_{PtOx}^{BoL/EoT}$ @ 1.8 A/cm^2).

comparable data in the literature exist, i.e. data that explicitly represents the half cell potential dependency of voltage losses attributed to PtOx-formation. Commonly, in papers investigating

PtOx, the accumulated charge measured in the PtOx reduction peak of a CV is used for oxide quantification [48–50, 68]. In all these works, the amount of PtOx increases with increasing half cell potential. This suggests that the PtOx overpotential would increase with half cell potential, too - and contradicts the observed maximum in Fig. 5. The authors believe that the increase of the PtOx overvoltage between 750 mV and 820 mV half cell potential is caused by higher kinetic loss due to an increasing oxide coverage of the catalyst particles [17, 69] and an increased loss from electron transport through (subsurface) oxides. Accordingly, the increase of oxide overvoltage with increasing half cell potential, arises not uniquely from kinetic oxide losses, but at least partially from Ohmic oxide losses, which also depend on current density. Consequently, the decrease of the PtOx losses at voltages higher than 820 mV represents lower kinetic and electronic losses from PtOx that arise from lower current densities (even though increasing Oxide loadings might further increase, as shown in [48–50]).

At half cell potentials lower than 750 mV η_{PtOx} seems to level off to a finite value. We speculate that this 10 mV-offset is related to the adsorption of anions from the ionomer on the catalyst surface. As Jinnouchi et al. showed by DFT simulations for Pt(111), adsorption of sulfate containing anions is thermodynamically favored between half cell potentials of 400 and 780 mV. These adsorbates suppress the oxide formation, poison the catalyst and result in an inhibition of the ORR [44, 69]. Accordingly, the authors believe that the "PtOx free" polarization curve has not only reduced losses from PtOx, but is also not impacted (or at least less impacted) from anion adsorption. This hypothesis is potentially in line with the findings of [70] about the regeneration of sulfonate adsorbates.

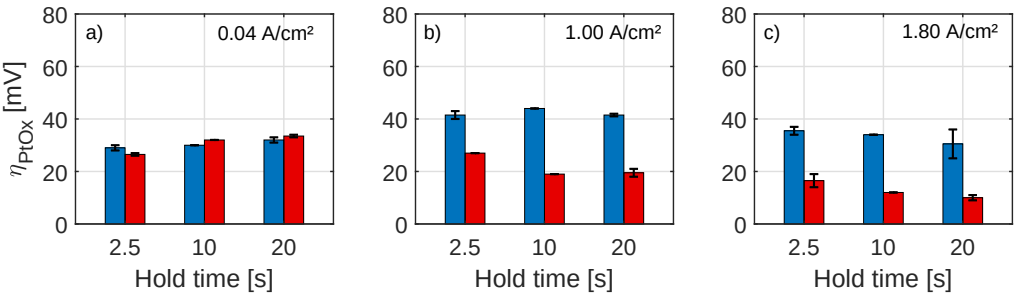

Figure 6: Overview of the averaged BoL (blue) and EoT (red) PtOx overvoltages at 0.04 (a), 1.0 (b) and 1.8 A/cm^2 (c).

Fig. 6 shows the measured PtOx related overvoltages at 0.04, 1.0 and 1.8 A/cm^2 at BoL and EoT extracted from Fig.5b . At 0.04 A/cm^2 (Fig. 6a) it can be seen that almost the same PtOx-related overvoltages are obtained at BoL and EoT independent of the chosen hold time. In Fig. 6b and c, the overvoltages at 1.0 A/cm^2 respectively at 1.8 A/cm^2 are shown. At these current densities η_{PtOx} is reduced significantly at EoT due to decreased half cell potential at higher current densities. And as the the activity decreases with increasing hold time (see Fig. 4) lower half cell potentials are obtained at EoT. Consequently, the reduction of η_{PtOx} is more severe if the hold time is increased from 2.5 to 10 s. But no further reduction of η_{PtOx} is obtained for a hold time of 20 s, as comparable activity losses are measured for hold times of 10 and 20 s. (see Fig. 4).

3.4. Break down of degradation-caused voltage losses

In this section the difference between the different overvoltages defined in section 2.3 at BoL and at EoT obtained for the three ASTs are compared to each other. The data described in the sections before are used to break down these losses into the different contributors of section 2.3 and the origin of the unassigned voltage loss is discussed.

Fig. 7a represents the equilibrium polarization curves at BoL and EoT for differently aged samples. In the Fig. 7b-d, the break down of the measured degradation related voltage losses at 0.04, 1.0 and 1.8 A/cm^2 following the equations 8-16 is depicted. In general one can see the following: As the HFR did not show significant changes over life (Fig. 3a-c), additional HFR-related voltage losses (according to eq. 12) are absent. The same is true for oxygen transport related losses, as the oxygen transport resistance was stable, too (Fig. 3g-i). Oppositely, the cathode proton resistance did show some improvement for all variants of the AST (Fig. 3d-f). This improvement is converted with the help of equation 13 and leads to negative voltage loss changes. PtOx-losses were seen to be reduced at EoT in Fig. 6 for all but the smallest currents. The work of Zago et al. also shows, that the catalyst activity is less influenced by PtOx for aged samples [44].

Accordingly, in Fig. 7c-d the difference is also counted as gain (bars heading negative). Increases in the voltage losses arise majorly from a reduction in activity, whereby $ECSA$ and SA contribute almost equally. The related bars are heading up, starting below zero at the value of total gain. The gap between the upper end of the $ECSA$-related voltage losses and the black tick marks the additional unassigned voltage losses at EoT. They will be discussed in the end of this section, when the impact of current density and hold time was rationalized. According to eq. 9 and 11 that $ECSA$

and SA related voltage losses are independent of current density and therefore constant in Fig. 7b-d. Increasing gains (with increasing current density) arise on the one hand from the trend in cathode proton losses with hold time. But no clear trend can be identified given the error bar of the cathode proton resistance (Fig. 3d-f). On the other hand, increasing gains (with increasing current density) arise from reduced oxide-related voltage losses. The root cause is simply a reduced oxide formation with decreasing half cell potential EoT, as shown in Fig. 5b. Thereby, the PtOx-gain is almost identical for 1.0 and 1.8 A/cm^2, simply due to the curvature of the oxide voltage losses with half cell potential (Fig. 5b - compare highlighted marks at 1.0 and 1.8 A/cm^2 BoL and EoT). On the other hand, the gain from a reduced cathode proton resistance also increases due its direct dependence on current density (eq. 13).

Discussing the impact of hold times, it is evident, that the total losses (black ticks) increase from 2.5 to 10 s. The outcome of the AST with 20 s hold time is then very close to the AST with 10 s hold - hardly larger than the error bar ($\sim$ 5 mV). This result is in line with earlier studies [11, 63], which found that ASTs with the same upper potential limit tend to the same EoT voltage losses. As expected, $ECSA$ and SA losses increase from 2.5 to 10 s, but not further when the hold time is 20 s. Regarding the trend in the PtOx-related voltage losses, one can see the lowest gain for the AST with 2.5 s hold time due to the higher EoT half cell potential. It seems that there is a little less gain in the case of 20 s hold time. However, this potentially unexpected difference between the ASTs with 10 and 20 s hold time is in the order of 5 mV and therefore pretty small. Nonetheless, it might point to slightly different EoT states of the samples - evidently particle size and shape have a tremendous impact on PtOx build-up [42, 43].

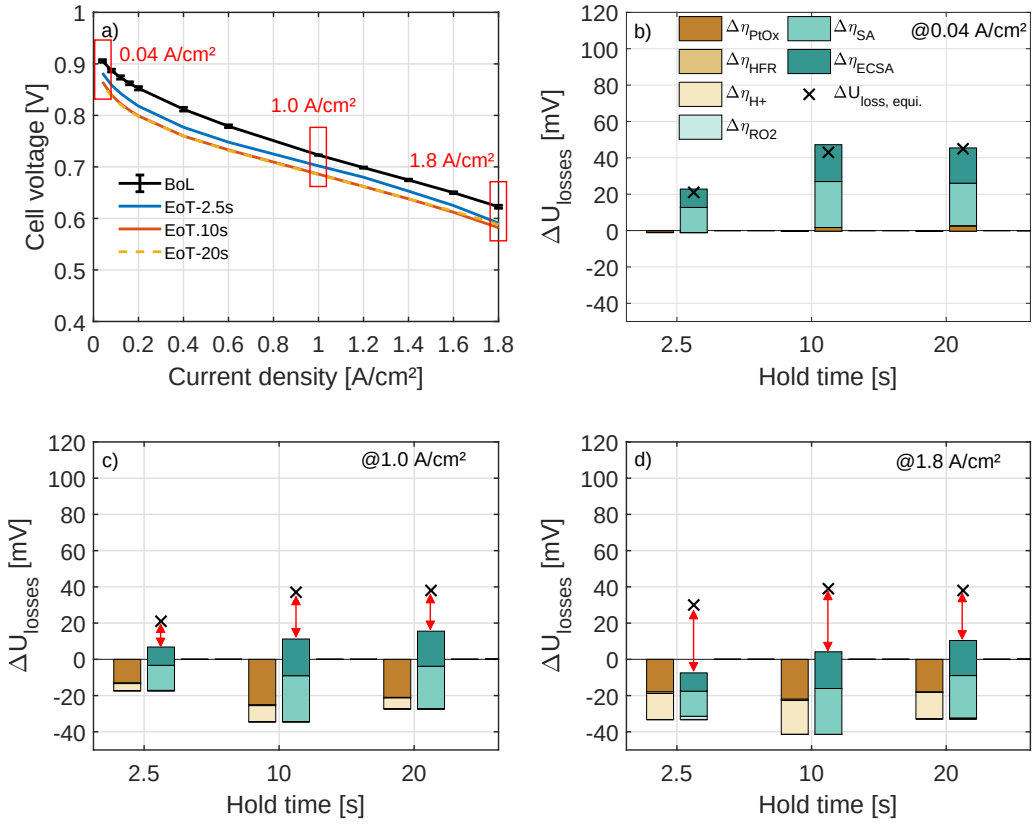

Figure 7: a) Averaged begin-of-life polarization curve and the obtained end-of-test polarization curves for the differently degraded samples ; b-d) Break down of the additional voltage losses at end-of-test at 0.04 (b), 1.0 (c) and 1.8 A/cm^2 (d)into the different contributors introduced in section 2.3.

In the end, the increase in unassigned voltage loss shall be discussed. Evidently, the loss is negligible at 0.04 A/cm^2 and increases with current density up to 35 mV. This insight is surprising, as the almost perfect vertical shift in the polarization curves EoT (Fig. 7a) suggests that degradation trivially causes activity losses only. However, if the PtOx related voltage losses are taken into account, unassigned losses remain or rather turn out larger than without considering PtOx.

Earlier, others have identified an unassigned voltage loss, too [30, 34–36]. However, in the current work the discussion of the unassigned voltage loss is based on the direct determination of the oxygen transport resistance and PtOx-related voltage losses. Accordingly, with this additional diagnostic

information, the often argued "increased oxygen transport resistance EoT" can be excluded as no change in oxygen transport resistance over the course of AST-testing is seen (Fig. 3g-i). A similar argument is derived in [8] derived from the comparison of stationary limiting currents at BoL and EoT. Two hypotheses seem more plausible to explain the unassigned voltage loss. The first hypothesis bases on an increased Tafel slope over the course of AST testing. Support of this idea arises from Fig. 8, which displays the unassigned voltage losses as a function of half cell potential at EoT. Indeed, a linear increase with half cell potential is seen. Therefore, the unassigned losses could be

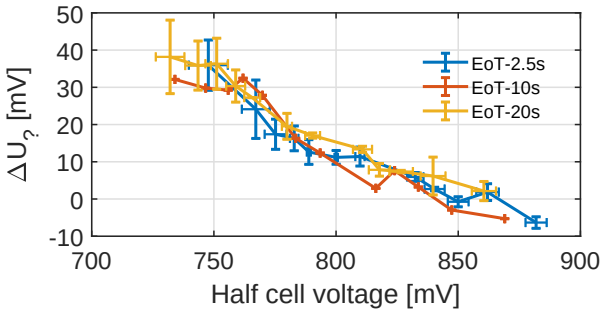

Figure 8: $\Delta\eta_?$ as function of the half cell potential EoT.

caused by an disregarded increase of the Tafel slope at EoT. This increase will lead to an steeper slope of the polarization curve and consequently the unassigned voltage losses would be reduced. However, assuming an increasing Tafel slope is counter intuitive as PtCo is known to exhibit a larger Tafel slope compared to Pt [71–73]. But likely the catalyst is more Pt-like at EoT due to leaching and accordingly should have lower Tafel slope at EoT compared to BoL - not larger.

The second hypothesis that might be plausible bases on catalyst poisoning due to sulfonate adsorption on the catalyst surface [74, 75]. Indeed, Kodama et al. found an increasing voltage loss from Nafion at Pt with decreasing half cell potential (Fig. 6 in [76]). Accordingly, at EoT more sulfonate adsorption losses could be expected at a given current. This expectation can be roughly quantified: Reading from Fig. 6 in [76], the losses from Nafion at Pt increase from $\sim$ 40 mV at a half cell potential of $\sim$900 mV to $\sim$60 mV at a half cell potential of $\sim$700 mV. This means at least a voltage loss of $\sim$10 mV can be attributed to the interaction between Nafion and the catalyst if there is a reduction of the half cell potential of 100 mV. Fig. 5b in this work shows, that the half cell potential at 1.8 A/cm^2 decreases from $\sim$800 mV to $\sim$700 mV over the cause of AST-testing (for all ASTs). This decrease of half cell potential yields 35 mV of unassigned loss (Fig. 8), which

is indeed more than the 10 mV expected from [76]. Nevertheless, one should also be aware that [76] is a study of Nafion on Pt(111) in an RDE-setup and therefore a considerably different system.

4. Conclusion

In this work, PEM-FC cathodes containing $PtCo$ catalyst, degraded with square wave accelerated stress tests of varying hold time, were analyzed with a dedicated diagnostic procedure. For every individual load point, the oxygen transport resistance and voltage losses due to the formation of $PtOx$ were obtained in addition to commonly measured electrochemical active surface area, high frequency as well as proton transport resistance. These data were used to break down the end-of-test voltage losses into six different contributors.

The high frequency resistance and the oxygen mass transport resistances shows no significant changes end-of-test. Consequently, no performance loss was attributed to an increased mass transport or to an increased Ohmic resistance end-of-test. In contrast, the proton resistance decreased for the analyzed samples, leading to performance gains after the accelerated stress tests. This behavior can be explained by a loss of carbon, leading to an increased volumetric ionomer content. As the electrochemical active surface area and the specific activity were reduced due to degradation, activity related performance losses are obtained. The $PtOx$ related losses are decreased at end-of-test, except at the smallest current densities. Most noticeably, it was shown that $PtOx$-related voltage losses show almost the same dependency on half cell voltage for all begin- and end-of-test samples. Taking all these different contributors into account, additional unassigned voltage losses remain.

Interestingly, the unassigned voltage loss was not only present at highest current densities as found elsewhere [30, 34, 36], but showed a steady increase with current density. When plotting it against half cell voltage, it was found to even be independent from the accelerated stress tests, or in other words: The unassigned voltage loss at end-of-test showed the same linear increase with cathode overvoltage for all accelerated stress tests. We speculate that the origin of the unassigned loss might arise from ionomer adsorption that, based on an earlier publication, depends on half cell voltage [76]. In the end it can not be in scope of membrane electrode assembly testing to unambiguously identify the root cause of the unassigned voltage loss, but with this new diagnostic procedure we believe to have made a good attempt in revealing its true impact.

Acknowledgements

We would like to thank Bianca Bauer and Yannis Fischer for help with the experimental work.

Appendix A

For the experiments a 5 cm^2 MEA-design based on the studies of Baker and Caulk [52] with a gas flow field of 50 cm^2 shown in Fig 9 and an active MEA area of 5 cm^2(Fig 10: MEA arranged on the flow field) are used.

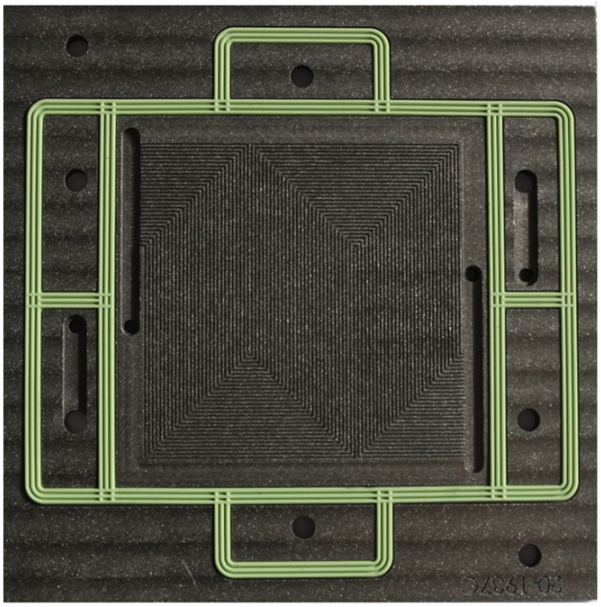

Figure 9: Flow-field-design based on the studies of Baker and Caulk [52].

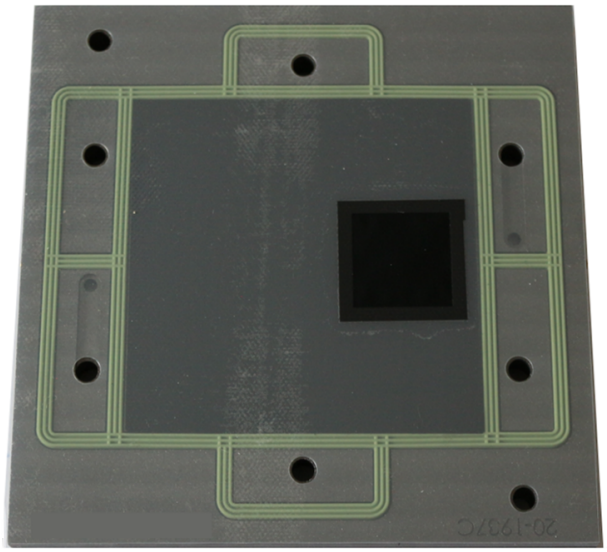

Figure 10: Flow-field with used GDL and 5 cm^2 MEA.

Appendix B

The high frequency resistance and the cathode ionomer resistance are determined by analyzing the recorded impedance spectra between 50 Hz and 30 kHz. Therefore a transmission line model derived from Makharia et al. [56] is used to fit the measured data. With this fit the HFR can be extracted by determing the high frequency intercept on the real impedance axis and the R_{H+} is extracted from the 45 ° branch of the fit (Fig 11).

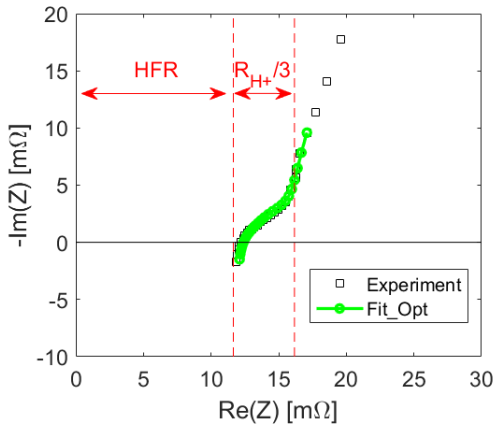

Figure 11: Fit of the measured impedance spectra and determination of the high frequency resistance and cathode ionomer resistance according to [56].

References

[1] S. Rasouli, R. A. Ortiz Godoy, Z. Yang, M. Gummalla, S. C. Ball, D. Myers, P. J. Ferreira, Surface Area Loss Mechanisms of Pt3Co Nanocatalysts in Proton Exchange Membrane Fuel Cells, Journal of Power Sources 343 (2017) 571–579. doi:10.1016/j.jpowsour.2017.01.058.

[2] Y. Cai, J. M. Ziegelbauer, A. M. Baker, W. Gu, R. S. Kukreja, A. Kongkanand, M. F. Mathias, R. Mukundan, R. L. Borup, Electrode Edge Cobalt Cation Migration in an Operating Fuel Cell: An In Situ Micro-X-ray Fluorescence Study, Journal of The Electrochemical Society 165 (6) (2018) F3132–F3138. doi:10.1149/2.0201806jes.

[3] R. L. Borup, R. Mukundan, D. Spernjak, D. A. Langlois, D. Torraco, K. L. More, R. Ahluwalia, S. Arisetty, L. Guétaz, Invited: Electrocatalyst Layer Degradation of PEM Fuel Cells, ECS Meeting Abstracts (2014). doi:10.1149/ma2014-02/21/1201.

[4] R. L. Borup, R. Mukundan, D. Spernjak, Y. S. Kim, D. A. Langlois, K. L. More, R. Ahluwalia, S. Arisetty, G. Maranzana, O. Lottin, PEM Fuel Cell MEA Structure Degradation, ECS Meeting Abstracts (2014). doi:10.1149/ma2014-01/18/788.

[5] J. Wu, X. Z. Yuan, J. J. Martin, H. Wang, J. Zhang, J. Shen, S. Wu, W. Merida, A review of PEM fuel cell durability: Degradation mechanisms and mitigation strategies, Journal of Power Sources 184 (1) (2008) 104–119. doi:10.1016/j.jpowsour.2008.06.006.

[6] P. Schneider, C. Sadeler, A.-C. Scherzer, N. Zamel, D. Gerteisen, Fast and Reliable State-of-Health Model of a PEM Cathode Catalyst Layer, Journal of The Electrochemical Society 166 (4) (2019) F322–F333. doi:10.1149/2.0881904jes.

[7] T. Jahnke, G. A. Futter, A. Baricci, C. Rabissi, A. Casalegno, Physical Modeling of Catalyst Degradation in Low Temperature Fuel Cells: Platinum Oxidation, Dissolution, Particle Growth and Platinum Band Formation, Journal of The Electrochemical Society 167 (1) (2019) 013523. doi:10.1149/2.0232001JES.

[8] G. S. Harzer, J. N. Schwämmlein, A. M. Damjanović, S. Ghosh, H. A. Gasteiger, Cathode Loading Impact on Voltage Cycling Induced PEMFC Degradation: A Voltage Loss Analysis, Journal of The Electrochemical Society 165 (6) (2018) F3118–F3131. doi:10.1149/2.0161806jes.

[9] A. Kneer, N. Wagner, A Semi-Empirical Catalyst Degradation Model Based on Voltage Cycling under Automotive Operating Conditions in PEM Fuel Cells, Journal of The Electrochemical Society 166 (2) (2019) F120–F127. doi:10.1149/2.0641902jes.

[10] A. A. Topalov, S. Cherevko, A. R. Zeradjanin, J. C. Meier, I. Katsounaros, K. J. J. Mayrhofer, Towards a comprehensive understanding of platinum dissolution in acidic media, Chem. Sci. 5 (2) (2014) 631–638. doi:10.1039/C3SC52411F.

[11] P. Zihrul, I. Hartung, S. Kirsch, G. Huebner, F. Hasché, H. A. Gasteiger, Voltage Cycling Induced Losses in Electrochemically Active Surface Area and in H2 /Air-Performance of PEM Fuel Cells, Journal of The Electrochemical Society 163 (6) (2016) F492–F498. doi:10.1149/2.0561606jes.

[12] N. Yousfi-Steiner, P. Moçotéguy, D. Candusso, D. Hissel, A review on polymer electrolyte membrane fuel cell catalyst degradation and starvation issues: Causes, consequences and diagnostic for mitigation, Journal of Power Sources 194 (1) (2009) 130–145. doi:10.1016/j.jpowsour.2009.03.060.

[13] W. Vielstich (Ed.), Handbook of fuel cells: Fundamentals, technology and applications, Wiley Interscience, Hoboken, NJ, 2010. doi:10.1002/9780470974001.

[14] F. A. de Bruijn, V. A. T. Dam, G. J. M. Janssen, Review: Durability and Degradation Issues of PEM Fuel Cell Components, Fuel Cells 8 (1) (2008) 3–22. doi:10.1002/fuce.200700053.

[15] S. ZHANG, X. YUAN, H. WANG, W. MERIDA, H. ZHU, J. SHEN, S. WU, J. ZHANG, A review of accelerated stress tests of MEA durability in PEM fuel cells, International Journal of Hydrogen Energy 34 (1) (2009) 388–404. doi:10.1016/j.ijhydene.2008.10.012.

[16] N. Macauley, R. Mukundan, D. A. Langlois, K. C. Neyerlin, S. S. Kocha, K. L. More, M. Odgaard, R. L. Borup, Durability of PtCo/C Cathode Catalyst Layers Subjected to Accelerated Stress Testing, ECS Transactions 75 (14) (2016) 281–287. doi:10.1149/07514.0281ecst.

[17] D. D. Papadias, R. K. Ahluwalia, N. Kariuki, D. Myers, K. L. More, D. A. Cullen, B. T. Sneed, K. C. Neyerlin, R. Mukundan, R. L. Borup, Durability of Pt-Co Alloy Polymer Electrolyte Fuel Cell Cathode Catalysts under Accelerated Stress Tests, Journal of The Electrochemical Society 165 (6) (2018) F3166–F3177. doi:10.1149/2.0171806jes.

[18] J. Hou, M. Yang, C. Ke, G. Wei, C. Priest, Z. Qiao, G. Wu, J. Zhang, Platinum-group-metal catalysts for proton exchange membrane fuel cells: From catalyst design to electrode structure optimization, EnergyChem 2 (1) (2020) 100023. doi:10.1016/j.enchem.2019.100023.

[19] M. Oezaslan, F. Hasché, P. Strasser, Pt-Based Core–Shell Catalyst Architectures for Oxygen Fuel Cell Electrodes, The Journal of Physical Chemistry Letters 4 (19) (2013) 3273–3291. doi:10.1021/jz4014135.

[20] S. Chen, H. A. Gasteiger, K. Hayakawa, T. Tada, Y. Shao-Horn, Platinum-Alloy Cathode Catalyst Degradation in Proton Exchange Membrane Fuel Cells: Nanometer-Scale Compositional and Morphological Changes, Journal of The Electrochemical Society 157 (1) (2010) A82. doi:10.1149/1.3258275.

[21] F. Jiang, F. Zhu, F. Yang, X. Yan, A. Wu, L. Luo, X. Li, J. Zhang, Comparative Investigation on the Activity Degradation Mechanism of Pt/C and PtCo/C Electrocatalysts in PEMFCs during the Accelerate Degradation Process Characterized by an in Situ X-ray Absorption Fine Structure, ACS Catalysis 10 (1) (2019) 604–612. doi:10.1021/acscatal.9b04598.

[22] Y. Cai, A. Kongkanand, W. Gu, T. E. Moylan, Effects of Cobalt Cation on Low Pt-loaded PEM Fuel Cell Performance, ECS Transactions 69 (17) (2015) 1047–1061. doi:10.1149/06917.1047ecst.

[23] A. Kusoglu, A. Z. Weber, New Insights into Perfluorinated Sulfonic-Acid Ionomers, Chemical reviews 117 (3) (2017) 987–1104. doi:10.1021/acs.chemrev.6b00159.

[24] S. Jeon, J. Lee, G. M. Rios, H.-J. Kim, S.-Y. Lee, E. Cho, T.-H. Lim, J. Hyun Jang, Effect of ionomer content and relative humidity on polymer electrolyte membrane fuel cell (PEMFC) performance of membrane-electrode assemblies (MEAs) prepared by decal transfer method, International Journal of Hydrogen Energy 35 (18) (2010) 9678–9686. doi:10.1016/j.ijhydene.2010.06.044.

[25] J. Zhang, Y. Tang, C. Song, Z. Xia, H. Li, H. Wang, J. Zhang, PEM fuel cell relative humidity (RH) and its effect on performance at high temperatures, Electrochimica Acta 53 (16) (2008) 5315–5321. doi:10.1016/j.electacta.2008.02.074.

[26] M. M. Mench, E. C. Kumbur, T. N. Veziroglu, Polymer electrolyte fuel cell degradation, Academic Press, Amsterdam, 2012.

[27] A. P. Young, J. Stumper, E. Gyenge, Characterizing the Structural Degradation in a PEMFC Cathode Catalyst Layer: Carbon Corrosion, Journal of The Electrochemical Society 156 (8) (2009) B913. doi:10.1149/1.3139963.

[28] J. C. Meier, C. Galeano, I. Katsounaros, A. A. Topalov, A. Kostka, F. Schüth, K. J. J. Mayrhofer, Degradation Mechanisms of Pt/C Fuel Cell Catalysts under Simulated Start–Stop Conditions, ACS Catalysis 2 (5) (2012) 832–843. doi:10.1021/cs300024h.

[29] H. Schulenburg, B. Schwanitz, N. Linse, G. G. Scherer, A. Wokaun, J. Krbanjevic, R. Grothausmann, I. Manke, 3D Imaging of Catalyst Support Corrosion in Polymer Electrolyte Fuel Cells, The Journal of Physical Chemistry C 115 (29) (2011) 14236–14243. doi:10.1021/jp203016u.

[30] T. A. Greszler, D. Caulk, P. Sinha, The Impact of Platinum Loading on Oxygen Transport Resistance, Journal of The Electrochemical Society 159 (12) (2012) F831–F840. doi:10.1149/2.061212jes.

[31] A. Kongkanand, M. F. Mathias, The Priority and Challenge of High-Power Performance of Low-Platinum Proton-Exchange Membrane Fuel Cells, The journal of physical chemistry letters 7 (7) (2016) 1127–1137. doi:10.1021/acs.jpclett.6b00216.

[32] T. Satake, Y. Tabe, T. Chikahisa, Analysis of Oxygen Transport Resistances in the Catalyst Layers with Different Carbon Supports in PEFC, ECS Transactions 86 (13) (2018) 171–178. doi:10.1149/08613.0171ecst.

[33] N. Nonoyama, S. Okazaki, A. Z. Weber, Y. Ikogi, T. Yoshida, Analysis of Oxygen-Transport Diffusion Resistance in Proton-Exchange-Membrane Fuel Cells, Journal of The Electrochemical Society 158 (4) (2011) B416. doi:10.1149/1.3546038.

[34] A. Orfanidi, P. Madkikar, H. A. El-Sayed, G. S. Harzer, T. Kratky, H. A. Gasteiger, The Key to High Performance Low Pt Loaded Electrodes, Journal of The Electrochemical Society 164 (4) (2017) F418–F426. doi:10.1149/2.1621704jes.

[35] A. Kneer, J. Jankovic, D. Susac, A. Putz, N. Wagner, M. Sabharwal, M. Secanell, Correlation of Changes in Electrochemical and Structural Parameters due to Voltage Cycling Induced Degradation in PEM Fuel Cells, Journal of The Electrochemical Society 165 (6) (2018) F3241–F3250. doi:10.1149/2.0271806jes.

[36] J. P. Owejan, J. E. Owejan, W. Gu, Impact of Platinum Loading and Catalyst Layer Structure on PEMFC Performance, Journal of The Electrochemical Society 160 (8) (2013) F824–F833. doi:10.1149/2.072308jes.

[37] M. Markiewicz, C. Zalitis, A. Kucernak, Performance measurements and modelling of the ORR on fuel cell electrocatalysts – the modified double trap model, Electrochimica Acta 179 (2015) 126–136. doi:10.1016/j.electacta.2015.04.066.

[38] N. P. Subramanian, T. A. Greszler, J. ZHANG, W. Gu, R. Makharia, J. ZHANG, Pt-Oxide Coverage-Dependent Oxygen Reduction Reaction (ORR) Kinetics, Journal of The Electrochemical Society 159 (5) (2012) B531–B540. doi:10.1149/2.088205jes.

[39] S. Jomori, N. Nonoyama, T. Yoshida, Analysis and modeling of PEMFC degradation: Effect on oxygen transport, Journal of Power Sources 215 (2012) 18–27. doi:10.1016/j.jpowsour.2012.04.069.

[40] A. Z. Weber, A. Kusoglu, Unexplained transport resistances for low-loaded fuel-cell catalyst layers, J. Mater. Chem. A 2 (41) (2014) 17207–17211. doi:10.1039/C4TA02952F.

[41] J. X. Wang, N. M. Markovic, R. R. Adzic, Kinetic Analysis of Oxygen Reduction on Pt(111) in Acid Solutions: Intrinsic Kinetic Parameters and Anion Adsorption Effects, The Journal of Physical Chemistry B 108 (13) (2004) 4127–4133. doi:10.1021/jp037593v.

[42] D. Fantauzzi, S. Krick Calderón, J. E. Mueller, M. Grabau, C. Papp, H.-P. Steinrück, T. P. Senftle, A. C. T. van Duin, T. Jacob, Growth of Stable Surface Oxides on Pt(111) at Near-Ambient Pressures, Angewandte Chemie 129 (10) (2017) 2638–2642. doi:10.1002/ange.201609317.

[43] B. Kirchhoff, L. Braunwarth, C. Jung, H. Jónsson, D. Fantauzzi, T. Jacob, Simulations of the Oxidation and Degradation of Platinum Electrocatalysts, Small (Weinheim an der Bergstrasse, Germany) 16 (5) (2020) e1905159. doi:10.1002/smll.201905159.

[44] M. Zago, A. Baricci, A. Bisello, T. Jahnke, H. Yu, R. Maric, P. Zelenay, A. Casalegno, Experimental analysis of recoverable performance loss induced by platinum oxide formation at the polymer electrolyte membrane fuel cell cathode, Journal of Power Sources 455 (2020) 227990. doi:10.1016/j.jpowsour.2020.227990.

[45] F. A. Uribe, T. A. Zawodzinski, A study of polymer electrolyte fuel cell performance at high voltages. Dependence on cathode catalyst layer composition and on voltage conditioning, Electrochimica Acta 47 (22-23) (2002) 3799–3806. doi:10.1016/S0013-4686(02)00350-X.

[46] H. Neff, S. Henkel, E. Hartmannsgruber, E. Steinbeiss, W. Michalke, K. Steenbeck, H. G. Schmidt, Structural, optical, and electronic properties of magnetron–sputtered platinum oxide films, Journal of Applied Physics 79 (10) (1996) 7672–7675. doi:10.1063/1.362341.

[47] L. Zhu, S. Kapoor, Q. Parry, A. Nahata, A. V. Virkar, Oxidation/reduction studies on nanoporous platinum films by electrical resistance measurements, Journal of Power Sources 269 (2014) 621–631. doi:10.1016/j.jpowsour.2014.07.039.

[48] S. Arisetty, Y. Liu, W. Gu, M. Mathias, Modeling Platinum Oxide Growth of PEMFC Cathode Catalysts, ECS Transactions 69 (17) (2015) 273–289. doi:10.1149/06917.0273ecst.

[49] B. E. Conway, B. Barnett, H. Angerstein-Kozlowska, B. V. Tilak, A surface–electrochemical basis for the direct logarithmic growth law for initial stages of extension of anodic oxide films formed at noble metals, The Journal of chemical physics 93 (11) (1990) 8361–8373. doi:10.1063/1.459319.

[50] M. Alsabet, M. Grden, G. Jerkiewicz, Comprehensive study of the growth of thin oxide layers on Pt electrodes under well-defined temperature, potential, and time conditions, Journal of Electroanalytical Chemistry 589 (1) (2006) 120–127. doi:10.1016/j.jelechem.2006.01.022.

[51] A. Kongkanand, J. M. Ziegelbauer, Surface Platinum Electrooxidation in the Presence of Oxygen, The Journal of Physical Chemistry C 116 (5) (2012) 3684–3693. doi:10.1021/jp211490a.

[52] D. R. Baker, D. A. Caulk, K. C. Neyerlin, M. W. Murphy, Measurement of Oxygen Transport Resistance in PEM Fuel Cells by Limiting Current Methods, Journal of The Electrochemical Society 156 (9) (2009) B991. doi:10.1149/1.3152226.

[53] R. Petrone, D. Hissel, M. C. Péra, D. Chamagne, R. Gouriveau, Accelerated stress test procedures for PEM fuel cells under actual load constraints: State-of-art and proposals, International Journal of Hydrogen Energy 40 (36) (2015) 12489–12505. doi:10.1016/j.ijhydene.2015.07.026.

[54] S. Stariha, N. Macauley, B. T. Sneed, D. Langlois, K. L. More, R. Mukundan, R. L. Borup, Recent Advances in Catalyst Accelerated Stress Tests for Polymer Electrolyte Membrane Fuel Cells, Journal of The Electrochemical Society 165 (7) (2018) F492–F501. doi:10.1149/2.0881807jes.

[55] M. Göbel, S. Kirsch, L. Schwarze, L. Schmidt, H. Scholz, J. Haußmann, M. Klages, J. Scholta, H. Markötter, S. Alrwashdeh, I. Manke, B. R. Müller, Transient limiting current measurements for characterization of gas diffusion layers, Journal of Power Sources 402 (2018) 237–245. doi:10.1016/j.jpowsour.2018.09.003.

[56] R. Makharia, M. F. Mathias, D. R. Baker, Measurement of Catalyst Layer Electrolyte Resistance in PEFCs Using Electrochemical Impedance Spectroscopy, Journal of The Electrochemical Society 152 (5) (2005) A970. doi:10.1149/1.1888367.

[57] K. C. Neyerlin, W. Gu, J. Jorne, H. A. Gasteiger, Determination of Catalyst Unique Parameters for the Oxygen Reduction Reaction in a PEMFC, Journal of The Electrochemical Society 153 (10) (2006) A1955. doi:10.1149/1.2266294.

[58] N. Macauley, D. D. Papadias, J. Fairweather, D. Spernjak, D. Langlois, R. Ahluwalia, K. L. More, R. Mukundan, R. L. Borup, Carbon Corrosion in PEM Fuel Cells and the Development of Accelerated Stress Tests, Journal of The Electrochemical Society 165 (6) (2018) F3148–F3160. doi:10.1149/2.0061806jes.

[59] K. H. Kangasniemi, D. A. Condit, T. D. Jarvi, Characterization of Vulcan Electrochemically Oxidized under Simulated PEM Fuel Cell Conditions, Journal of The Electrochemical Society 151 (4) (2004) E125. doi:10.1149/1.1649756.

[60] C. Takei, K. Kakinuma, K. Kawashima, K. Tashiro, M. Watanabe, M. Uchida, Load cycle durability of a graphitized carbon black-supported platinum catalyst in polymer electrolyte fuel cell cathodes, Journal of Power Sources 324 (2016) 729–737. doi:10.1016/j.jpowsour.2016.05.117.

[61] D. Gerteisen, Impact of Inhomogeneous Catalyst Layer Properties on Impedance Spectra of Polymer Electrolyte Membrane Fuel Cells, Journal of The Electrochemical Society 162 (14) (2015) F1431–F1438. doi:10.1149/2.0511514jes.

[62] Y. Wang, T. Liu, H. Sun, W. He, Y. Fan, S. Wang, Investigation of dry ionomer volume fraction in cathode catalyst layer under different relative humilities and nonuniform ionomer-gradient distributions for PEM fuel cells, Electrochimica Acta 353 (2020) 136491. doi:10.1016/j.electacta.2020.136491.

[63] A. Kneer, N. Wagner, C. Sadeler, A.-C. Scherzer, D. Gerteisen, Effect of Dwell Time and Scan Rate during Voltage Cycling on Catalyst Degradation in PEM Fuel Cells, Journal of The Electrochemical Society 165 (10) (2018) F805–F812. doi:10.1149/2.0651810jes.

[64] R. K. Ahluwalia, X. Wang, J.-K. Peng, N. N. Kariuki, D. J. Myers, S. Rasouli, P. J. Ferreira, Z. Yang, A. Martinez-Bonastre, D. Fongalland, J. Sharman, Durability of De-Alloyed Platinum-Nickel Cathode Catalyst in Low Platinum Loading Membrane-Electrode Assemblies Subjected to Accelerated Stress Tests, Journal of The Electrochemical Society 165 (6) (2018) F3316–F3327. doi:10.1149/2.0341806jes.

[65] M. Watanabe, H. Yano, D. A. Tryk, H. Uchida, Highly Durable and Active PtCo Alloy/Graphitized Carbon Black Cathode Catalysts by Controlled Deposition of Stabilized Pt Skin Layers, Journal of The Electrochemical Society 163 (6) (2016) F455–F463. doi:10.1149/2.0331606jes.

[66] E. Padgett, V. Yarlagadda, M. E. Holtz, M. Ko, B. D. A. Levin, R. S. Kukreja, J. M. Ziegelbauer, R. N. Andrews, J. Ilavsky, A. Kongkanand, D. A. Muller, Mitigation of PEM Fuel Cell Catalyst Degradation with Porous Carbon Supports, Journal of The Electrochemical Society 166 (4) (2019) F198–F207. doi:10.1149/2.0371904jes.

[67] H. Yano, M. Watanabe, A. Iiyama, H. Uchida, Particle-size effect of Pt cathode catalysts on durability in fuel cells, Nano Energy 29 (2016) 323–333. doi:10.1016/j.nanoen.2016.02.016.

[68] E. L. Redmond, B. P. Setzler, F. M. Alamgir, T. F. Fuller, Elucidating the oxide growth mechanism on platinum at the cathode in PEM fuel cells, Physical chemistry chemical physics : PCCP 16 (11) (2014) 5301–5311. doi:10.1039/c3cp54740j.

[69] R. Jinnouchi, T. Hatanaka, Y. Morimoto, M. Osawa, First principles study of sulfuric acid anion adsorption on a Pt(111) electrode, Physical chemistry chemical physics : PCCP 14 (9) (2012) 3208–3218. doi:10.1039/c2cp23172g.

[70] H. S. Choo, D. K. Chun, J. H. Lee, H. S. Shin, S. K. Lee, Y. S. Park, B. K. Ahn (Eds.), SAE 2015 World Congress & Exhibition // Performance Recovery of Fuel Cell Stack for FCEV, SAE Technical Paper Series, SAE International400 Commonwealth Drive, Warrendale, PA, United States, 2015. doi:10.4271/2015-01-1171.

[71] C. Zalitis, A. Kucernak, X. Lin, J. Sharman, Electrochemical Measurement of Intrinsic Oxygen Reduction Reaction Activity at High Current Densities as a Function of Particle Size for Pt 4–x Co x /C (x = 0, 1, 3) Catalysts, ACS Catalysis (2020) 4361–4376doi:10.1021/acscatal.9b04750.

[72] H. Yano, I. Arima, M. Watanabe, A. Iiyama, H. Uchida, Oxygen Reduction Activity and Durability of Ordered and Disordered Pt 3 Co Alloy Nanoparticle Catalysts at Practical Temperatures of Polymer Electrolyte Fuel Cells, Journal of The Electrochemical Society 164 (9) (2017) F966–F972. doi:10.1149/2.1141709jes.

[73] G. Sievers, S. Mueller, A. Quade, F. Steffen, S. Jakubith, A. Kruth, V. Brueser, Mesoporous Pt–Co oxygen reduction reaction (ORR) catalysts for low temperature proton exchange membrane fuel cell synthesized by alternating sputtering, Journal of Power Sources 268 (2014) 255–260. doi:10.1016/j.jpowsour.2014.06.013.

[74] J. Liu, Y. Huang, Oxygen Reduction Reaction on PtCo Nanocatalyst: (Bi)sulfate Anion Poisoning, Nanoscale research letters 13 (1) (2018) 156. doi:10.1186/s11671-018-2574-6.

[75] K. Kodama, A. Shinohara, N. Hasegawa, K. Shinozaki, R. Jinnouchi, T. Suzuki, T. Hatanaka, Y. Morimoto, Catalyst Poisoning Property of Sulfonimide Acid Ionomer on Pt (111) Surface, Journal of The Electrochemical Society 161 (5) (2014) F649–F652. doi:10.1149/2.051405jes.

[76] K. Kodama, A. Shinohara, R. Jinnouchi, Y. Morimoto, Strategies for Designing Ideal Pt/Ionomer Interfaces in Polymer Electrolyte Fuel Cells, Popularizing Fuel Cell Vehicles: Desiging and Controlling Electrochmeical Reactions in the MEA (49) (2018) 1–11.